J. Appl. Cryst. (1991). **24**, 571–575

Low-Angle X-ray Diffraction of Multilayered Structures

By H. Vanderstraeten, D. Neerinck, K. Temst and Y. Bruynseraede

Laboratorium voor Vaste Stof-Fysika en Magnetisme, Katholieke Universiteit Leuven, B-3001 Leuven, Belgium

and Eric E. Fullerton and Ivan K. Schuller

Physics Department–B019, University of California–San Diego, California 92093, USA

(*Received* 28 *September* 1990; *accepted* 4 *April* 1991)

Abstract

Low-angle X-ray diffraction profiles can provide detailed information about the multilayer periodicity and thickness of the individual layers that make up a multilayer. The effect of discrete and continuous random cumulative fluctuations of the layer thicknesses on the diffraction profiles of single films, bilayers and multilayers is discussed. It is shown that the calculated low-angle profiles of single films can distinguish between discrete and continuous thickness errors. In bilayers and multilayers, however, no difference between these thickness errors can be seen and only an overall thickness error may be extracted.

1. Introduction

Multilayers consist in general of two materials layered sequentially on top of each other. They have been proven to be very important for studies regarding new transport, superconducting, magnetic and elastic properties (Schuller, 1988). They can also be used as mirrors for radiation in the far UV and X-ray regions (Henke, Gullikson, Kerner, Oren & Blake, 1990; Mezei, 1988) where questions concerning the design (Spiller, 1988), stability and interdiffusion (Spaepen, 1988) and deviations from perfect growth (Spiller & Rosenbluth, 1986) are of primary interest.

Multilayers give rise to new periodicities at length scales longer than the atomic scale due to the imposed chemical modulation of a characteristic length Λ. X-ray diffraction is a unique technique for the analysis of the structure of these materials since it can provide detailed nondestructive information about Λ, the thickness of the individual layers (from the low-angle profiles around the zero-order Bragg reflections of the atomic spacings), and additionally about d_A and d_B, the lattice spacings of the constituent materials (from the high-angle profiles around the first- and higher-order Bragg reflections of d_A and d_B) (Segmüller & Blakeslee, 1973).

A multilayer is never perfect and deviations from the ideal structure have to be included in any structural modelling in order to explain quantitatively the experimental profiles. Various types of imperfections may be present. The lattice mismatch between the two materials or the amorphicity of one of the materials can give rise to fluctuations in the modulation wavelength of a continuous kind, and a variable number of atomic planes in the crystalline layers may cause discrete fluctuations of the thicknesses of the layers. Deviations from perfect crystallinity or amorphicity of the layers and interdiffusion can strongly influence the diffraction pattern and limit the number of Bragg reflections.

In this paper, we discuss the effect on the low-angle profiles of imperfections in multilayers consisting of immiscible materials. Since the structure within a layer is described by distances comparable with typical X-ray wavelengths used (1·54 Å), the effect of these cannot be observed at low angles. Therefore, the only types of imperfections we will discuss will be discrete or continuous cumulative fluctuations of the layer thicknesses.

These imperfections have proven to be essential elements in the explanation of the high-angle profiles. Continuous cumulative fluctuations annihilate the superlattice diffraction peaks in crystalline/amorphous systems (Sevenhans, Gijs, Bruynseraede, Homma & Schuller, 1986), and only a finite-size-limited Bragg reflection of the crystalline component is observed (see also Spiller, Segmüller, Rife & Haelbich 1980; Ziegler, Lepetre, Schuller & Spiller, 1986). Discrete roughness has been introduced to explain the peak broadening in crystalline/crystalline systems (Clemens & Gay, 1987; Locquet, Neerinck, Stockman, Bruynseraede & Schuller, 1989) and the number of finite-size peaks in crystalline/amorphous systems (Neerinck, Vanderstraeten *et al.*, 1990).

Here, the multilayer is considered as a one-dimensional stack, contrary to many workers in the field of X-ray optics who consider lateral non-cumulative roughnesses.

0021-8898/91/050571-05$03.00 © 1991 International Union of Crystallography

In §2, the experimental details of sample preparation and diffraction measurements are given. §3 will give a short overview of the formalisms used for calculating the low-angle profiles. The formalism we use will be treated in somewhat more detail. In §4, the effect of these errors on the low-angle profiles of a single layer, a bilayer and a multilayer will be discussed.

2. Experimental procedure

The Pb/Ge and Pb/Cu samples were prepared in a load-locked molecular beam epitaxy apparatus equipped with two electron beam guns. The evaporation rates were controlled using a quadrupole mass spectrometer in feedback mode (Sevenhans, Locquet & Bruynseraede, 1986). The liquid-nitrogen-cooled sapphire or silicon oxide substrates were exposed to the evaporant at pressures lower than 1·33 MPa. The top layer was always Ge or Cu, to prevent the Pb from oxidizing.

X-ray diffraction measurements in the θ–2θ mode were carried out on a computer-controlled 12 kW DMax II Rigaku rotating-anode Bragg–Brentano setup (goniometer circle radius 185 mm) using Cu $K\alpha$ radiation. The diffracted radiation was filtered with a flat pyrolytic monochromator. Extreme care was taken to position the sample surface coincident with the θ goniometer axis. All profiles were taken with a divergence slit of $\frac{1}{6}°$, a receiving slit of 0·3 mm and a scattering slit of $\frac{1}{2}°$.

3. Theoretical formalism

If the length scales probed in a diffraction experiment have a short coherence length, a kinematical approach is a good approximation. If, however, the coherence length is very long compared to the periods measured, a dynamical formalism, which takes the primary and secondary extinction effects into account, should be used. The latter approach must therefore be used in cases of, for instance, semiconductor superlattices which have a near-perfect crystalline quality on all length scales (Tapfer & Ploog, 1986), or in multilayers where the superstructure (not the structure of the constituent layers) is almost a perfect crystal in the growth direction. Since the superstructure is investigated at low angles, we have to use a dynamical formalism to simulate low-angle profiles. Furthermore, in the very low-angle-region refraction, absorption and total internal reflection at the surface can play a role. An optical formalism includes the latter effects and is equivalent with the dynamical theory (James, 1965).

Optical formalisms treat the multilayer as a stack of uniform layers of thicknesses t_A and t_B, with complex indices of refraction n_A and n_B. The structure within a layer is assumed to be homogeneous, which is a reasonable assumption given the length scales probed in low-angle diffraction. An introduction to the optical theory can be found in, for instance, Born & Wolf (1975). The reflection and transmission of a multilayer can be calculated using matrix methods, where each interface is characterized by a matrix and the multilayer by the product matrix, or a recursive use of the single-film formula (Underwood & Barbee, 1981; Spiller & Rosenbluth, 1986). In this latter calculation the reflectivity of an interface between the jth and $(j+1)$th material is expressed in terms of the Fresnel coefficients and the reflectivity of the interface below it (Underwood & Barbee, 1981):

$$R_{j,j+1} = \exp[-i(\pi/\lambda)(n_j^2 - \cos^2\theta)^{1/2}t_j] \times [(R_{j+1,j+2} + r_{j,j+1})/(R_{j+1,j+2}r_{j,j+1} + 1)], \quad (1)$$

where $r_{j,j+1}$ is the Fresnel reflection coefficient and $R_{j+1,j+2}$ the reflectivity. The prefactor includes the phase shift introduced by the jth layer. The calculation is started at medium n, the substrate, with $R_{n,n+1} = 0$ since the substrate is infinitely thick, and is applied recursively up to the sample surface where the total reflectance is given by $R_{1,2}$. The normalized reflected intensity can then be calculated as

$$I(\theta) = |R_{1,2}|^2. \quad (2)$$

In order to calculate the reflected intensity of a multilayer with random discrete and continuous fluctuations of the layer thicknesses, the ensemble average of the intensity must be taken over all these variables. Vidal & Vincent (1984) calculated a closed-form analytical expression for the average of the reflectivity and not the intensity, where they took the ensemble average over the continuous variable only. However, a closed-form analytical expression for the average of the *intensity* over *both* the discrete and continuous variables is not available. Therefore, we average numerically, where the layer thicknesses $t_{j,A}$ of material A in (1) are taken to fluctuate around an average t_A,

$$t_{j,A} = t_A + a_{j,d} + a_{j,c}, \quad (3)$$

and the variables $a_{j,c}$ are assumed to have a continuous Gaussian distribution with a width $\sigma_{A,c}$ and $a_{j,d}$ are distributed around a discrete Gaussian with a width $\sigma_{A,d}$, both around zero average, *i.e.*

$$P(a_{j,c}) = [1/\sigma_{A,c}(2\pi)^{1/2}]\exp(-a_{j,c}^2/2\sigma_{A,c}^2)$$

and (4)

$$P(a_{j,d}) = [1/\sigma_{A,d}(2\pi)^{1/2}]\exp(-a_{j,d}^2/2\sigma_{A,d}^2).$$

The step width of the discrete distribution is d_A, the atomic-planes spacing. The same conventions and equations hold for material B, where all indices A are to be replaced by B.

The total reflectance is calculated and summed for L_{av} multilayers, where each multilayer is built with the fluctuating thicknesses given by (3). This average reflectance is squared to give the intensity. This intensity is in turn averaged over N_{av} multilayers to give the average reflected intensity:

$$I = (1/N_{av}) \sum_{n=1}^{N_{av}} |(1/L_{av}) \sum_{l=1}^{L_{av}} R_{n,l}|^2. \qquad (5)$$

L_{av} and N_{av} have to be taken large enough so that the Gaussian populations [(4)] are accurately represented. This can be estimated from the numerical noise in the calculated profiles. If $L_{av} = 1$, only the intensity is averaged, thus taking only incoherent in-plane scattering into account, because there is no longer a phase relation between the two reflected waves. L_{av} should be larger than one, as previously shown by Neerinck, Temst *et al.* (1990), but its precise value does not matter if only a qualitative comparison with experiment is needed.

If $N_{av} = 1$, the incoherent scattering perpendicular to the layers is not included. Typically, $N_{av} = 200$ and $L_{av} = 20$.

It should be emphasized that the way the fluctuations in the thicknesses are taken into account assumes a cumulative type of disorder (Sevenhans, Gijs *et al.*, 1986). As a consequence, if the *j*th layer thickness has a spread σ, the distance $= \sum_{k=n-1}^{j} t_k$ between the top of this layer and the substrate has a spread $(n-j)^{1/2}\sigma$. Owing to this the first-order Bragg reflection of the superstructure shifts over a range σ, while the *j*th-order reflection shifts over a range $y^{1/2}\sigma$. The *j*th-order reflection will thus be broader than the first order, as opposed to non-cumulative disorder, which is equivalent to an effective Debye–Waller factor, which does not broaden the reflections (Spiller & Rosenbluth, 1986).

4. Discussion

A single thin layer of an amorphous material can have a continuous disorder due to roughness of the (amorphous) substrate and local fluctuations of the layer thickness. Fig. 1 shows the low-angle profile of a 300 Å Ge film on an SiO_2 substrate, evaporated at liquid-nitrogen temperature to ensure the amorphicity of the layer. The experimental curve (full line) is characteristic of continuous roughness: a monotonously decreasing intensity of the reflections. The distance between successive minima is connected to the thickness of the layer *via* a law similar to the Bragg law (in a kinematical approximation), $2t = \lambda/(\sin\theta_{j+1} - \sin\theta_j)$, where j is the order of the reflection. The simulation (dashed line) using the formalism outlined above is calculated with an average thickness of 294 Å and a spread $\sigma_c = 6$ Å and is in good qualitative agreement, *i.e.* it reproduces all important features, with the experiment. In order to have a good quantitative agreement, one should account for the finite size of the sample, the angular divergence of the X-ray beam and its spectral width. It is clear that an increase of σ_c decreases the peak intensities faster.

The roughness of a single thin film of a crystalline material is mainly discrete. Some continuous disorder due to substrate roughness and small deviations from perfect crystallinity of the layer may also be present. Fig. 2 shows the low-angle profile (full line) of a 240 Å Cu film on an SiO_2 substrate, sputtered at room temperature. The experimental curve shows a beating of the interference pattern, which has been explained by assuming a thin oxide layer on top of the Cu layer (Segmüller, 1973; Baribeau, 1990). We show that discrete roughness can also account for this effect. This can be understood qualitatively using the following argument. Neglecting refraction, the Bragg condition for a film consisting

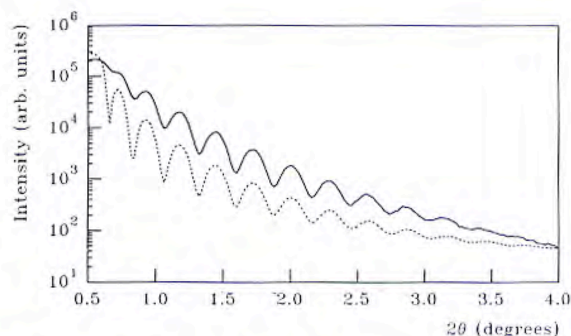

Fig. 1. Low-angle X-ray diffraction profile of an amorphous Ge(300 Å) single film. The experimental data (full line) were taken with a fixed divergence slit of $\frac{1}{6}°$. The simulation (dashed line) is calculated for a thickness of 296 Å and a fluctuation width $\sigma_c = 6$ Å.

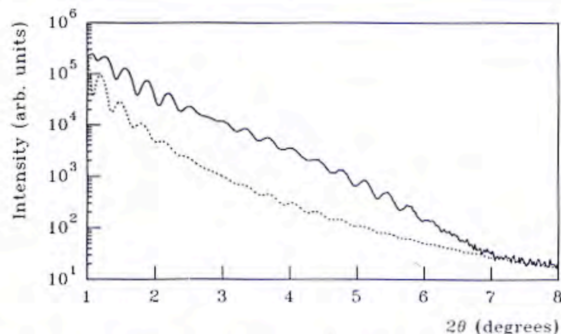

Fig. 2. Low-angle X-ray diffraction profile of a crystalline Cu single film. The experimental data (full line) were taken with a fixed divergence slit of $\frac{1}{6}°$. The simulation (dashed line) is calculated for a thickness of 240 Å, a discrete fluctuation width $\sigma_d = 16$ Å and a continuous fluctuation width $\sigma_c = 2$ Å.

of N average atomic planes separated by a distance d is given by

$$2Nd\sin\theta = n\lambda. \qquad (6)$$

At some places on the film, the layer consists of $N + 1$ atomic planes, and the diffraction peaks are out of phase with other places having N atomic planes at angle θ satisfying

$$2(N + 1)d\sin\theta = (n + 1/2)\lambda. \qquad (7)$$

Eliminating n between (1) and (2) gives $2(2d)\sin\theta = \lambda$. Layers with $N + j$ planes will have diffraction peaks out of phase with the N-plane layer at position θ given by $2(2jd)\sin\theta = \lambda$. Peak intensities vanish at small θ if j or σ_d is big. The final profile is determined by the relative probability between out-of-phase and in-phase domains, which is governed by the width of the Gaussian distribution. The dashed line in Fig. 2 shows a simulation for a Cu film with $d = 2{\cdot}084$ Å, $N = 115$, $\sigma_d = 16$ Å and $\sigma_c = 2$ Å. The main features of the experimental profile can be reproduced, except for the change in slope around $7°(2\theta)$, which is probably an instrumental artefact. However, the Cu film had a thin oxide overlayer, which also gives rise to the beating (Baribeau, 1990). In an attempt to separate the contributions of discrete disorder and an overlayer, we measured the surface topography of 500 Å Au films (which do not oxidize) deposited on mica (which allows an epitaxic growth) using a scanning tunnelling microscope. Although discrete steps were clearly observed, the flexibility of the mica foil masked the detection of possible discrete fluctuations in the X-ray diffraction profile. Further studies with epitaxic Au films on GaAs are currently being undertaken. At this point, we have to conclude that the theoretically predicted beating in the low-angle X-ray diffraction profile due to discrete roughness cannot be experimentally confirmed.

The bilayer profile is mainly controlled by the relative difference in refractive index of the two materials, which is related to the atomic density and the scattering power of the material. The profile of a Pb/Ge bilayer for instance will be dominated by the Pb single-film profile, while for Pb/Cu the profile will be determined by the total thickness of the bilayer, since the real parts of the indices of refraction are in this case almost equal.

Since the bilayer profile is determined not only by the individual layers of materials A and B, but also by the interference between them, it becomes very difficult to distinguish discrete from continuous roughness in the low-angle profile of a bilayer and only the overall roughness $\sigma = (\sigma_c^2 + \sigma_d^2)^{1/2}$ becomes important. Fig. 3 shows a simulation of a [Pb (277 Å)/Ge(283 Å)] bilayer calculated with a discrete roughness $\sigma_{d,\mathrm{Pb,Ge}} = 10$ Å (full line) and with a continuous roughness $\sigma_{c,\mathrm{Pb,Ge}} = 10$ Å (dashed line).

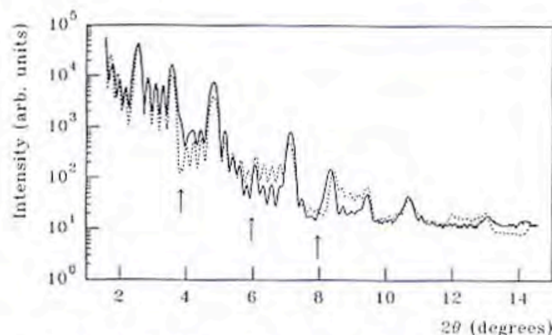

Fig. 4. Low-angle X-ray diffraction profile of a [Pb(45·4 Å)/Ge(29·5 Å)]$_5$ multilayer. The subscript indicates the number of bilayers. The arrows indicate the superimposed bilayer profile. The full line is the experimental curve, the dashed line the simulation, calculated with thicknesses $t_{\mathrm{Pb}} = 45{\cdot}2$ and $t_{\mathrm{Ge}} = 29{\cdot}2$ Å and fluctuations on the layer thicknesses $\sigma_{\mathrm{Pb}} = 1{\cdot}5$ and $\sigma_{\mathrm{Ge}} = 0{\cdot}5$ Å.

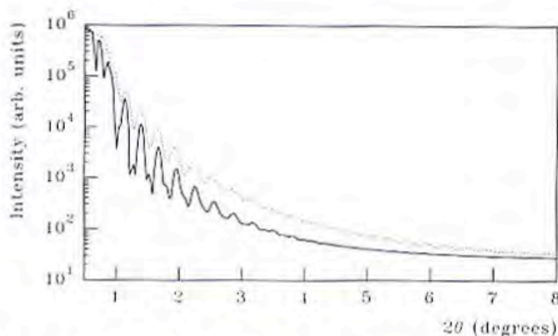

Fig. 3. Low-angle X-ray simulation of a [Pb(277 Å)/Ge(283 Å)] bilayer with a discrete roughness $\sigma_{d,\mathrm{Pb,Ge}} = 10$ Å (full line) and with a continuous roughness $\sigma_{c,\mathrm{Pb,Ge}} = 10$ Å (dashed line). The profiles are equal within 0·5%. The dotted line is a simulation for a Pb (277 Å) single film with $\sigma_{d,\mathrm{Pb}} = 10$ Å.

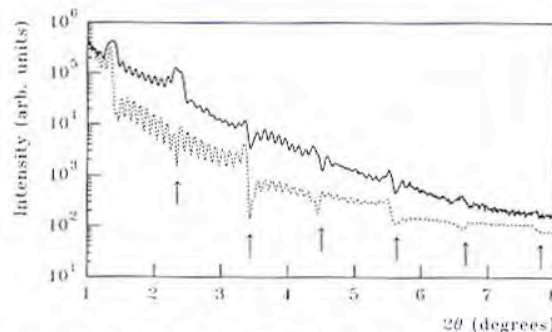

Fig. 5. Low-angle X-ray diffraction profile of a [Pb(40 Å)/Cu(40 Å)]$_{10}$ multilayer. The subscript indicates the number of bilayers. The arrows indicate the superimposed finite-size profile of a [Pb(40 Å)/Cu(40 Å)] bilayer. The full line is the experimental curve, the dashed line the simulation of a [Pb(42·9 Å)/Cu(37·5 Å)]$_{10}$ multilayer with fluctuations $\sigma_{\mathrm{Pb,Cu}} = 1{\cdot}5$ Å.

Both profiles are equal within 0·5%, although the single Pb(277 Å) layer profile with $\sigma_{d,Pb} = 10$ Å (dotted line) does show the characteristic behaviour for discrete roughness.

The multilayer profile consists of the product of the bilayer profile and the profile of a crystal with a periodicity Λ. If the multilayer is of sufficiently high quality, the bilayer profile can still be resolved, as is the case in Fig. 4, which shows the experimental low-angle profile (full line) of a $[Pb(45{\cdot}4\,Å)/Ge(29{\cdot}5\,Å)]_5$ (Neerinck, Vanderstraeten *et al.*, 1990) multilayer, evaporated at liquid-nitrogen temperature, consisting of five bilayers. This profile shows the finite-size-limited (only five unit cells) superperiod up to 12th order and the superimposed bilayer profile (the minima indicated by the arrows in the figure correspond to the minima of the bilayer profile), which is mainly determined by Pb, and thus gives a good estimate of the thickness of the Pb. The simulation (dashed line) is calculated for $t_{Pb} = 45{\cdot}2$, $t_{Ge} = 29{\cdot}2$, $\sigma_{Pb} = 1{\cdot}5$ and $\sigma_{Ge} = 0{\cdot}5$ Å. Fig. 5 shows the experimental diffraction profile (full line) of a $[Pb(40\,Å)/Cu(40\,Å)]_{10}$ multilayer (Neerinck, Temst *et al.*, 1990), again evaporated at liquid-nitrogen temperature. The $10 - 2 = 8$ finite-size multilayer peaks and the bilayer profile, which cuts into every superlattice peak, are clearly visible. The simulation (dashed line) is calculated for a $[Pb(42{\cdot}9\,Å)/Cu(37{\cdot}5\,Å)]_{10}$ multilayer with an overall roughness $\sigma = 1{\cdot}5$ Å on Pb and Cu. Additional information must be gained from the corresponding high-angle profile to distinguish between continuous and discrete roughness.

This work was supported by the Belgian Inter University Institute of Nuclear Sciences (IIKW), the Inter University Attraction Poles (IUAP) and Concerted Action (GOA) Programs at KU Leuven, and US DOE grant DE-FG03-87ER45332 at UCSD. Travel support was provided by NATO.

References

BARIBEAU, J. M. (1990). *Appl. Phys. Lett.* **57**, 1748–1750.

BORN, M. & WOLF, E. (1975). *Principles of Optics*. Oxford: Pergamon Press.

CLEMENS, B. M. & GAY, J. G. (1987). *Phys. Rev. B*, **35**, 9337–9340.

HENKE, B. L., GULLIKSON, E. M., KERNER, J., OREN, A. L. & BLAKE, R. L. (1990). *J. X-ray Sci. Technol.* **2**, 17–80.

JAMES, R. W. (1965). *The Optical Principles of the Diffraction of X-rays*. Cornell Univ. Press.

LOCQUET, J.-P., NEERINCK, D., STOCKMAN, L., BRUYNSERAEDE, Y. & SCHULLER, I. K. (1989). *Phys. Rev. B*, **39**, 13338–13342.

MEZEI, F. (1988). In *Physics, Fabrication and Applications of Multilayered Structures*, edited by P. DHEZ & C. WEISBUCH, pp. 310–336. New York, London: Plenum Press.

NEERINCK, D., TEMST, K., VANDERSTRAETEN, H., VAN HAESENDONCK, C., BRUYNSERAEDE, Y., GILABERT, A. & SCHULLER, I. K. (1990). *Mater. Res. Soc. Symp. Proc.* **160**, 599–604.

NEERINCK, D., VANDERSTRAETEN, H., STOCKMAN, L., LOCQUET, J.-P., BRUYNSERAEDE, Y. & SCHULLER, I. K. (1990). *J. Phys: Condens. Matter*, **2**, 4111–4118.

SCHULLER, I. K. (1988). In *Physics, Fabrication and Applications of Multilayered Structures*, edited by P. DHEZ & C. WEISBUCH, pp. 139–170. New York, London: Plenum Press.

SEGMÜLLER, A. (1973). *Thin Solid Films*, **18**, 287-294.

SEGMÜLLER, A. & BLAKESLEE, A. E. (1973). *J. Appl. Cryst.* **6**, 19-25.

SEVENHANS, W., GIJS, M., BRUYNSERAEDE, Y., HOMMA, H. & SCHULLER, I. K. (1986). *Phys. Rev. B*, **34**, 5955–5958.

SEVENHANS, W., LOCQUET, J.-P. & BRUYNSERAEDE, Y. (1986). *Rev. Sci. Instrum.* **57**, 937–940.

SPAEPEN, F. (1988). In *Physics, Fabrication and Applications of Multilayered Structures*, edited by P. DHEZ & C. WEISBUCH, pp. 199–214. New York, London: Plenum Press.

SPILLER, E. (1988). In *Physics, Fabrication and Applications of Multilayered Structures*, edited by P. DHEZ & C. WEISBUCH, pp. 271–310. New York, London: Plenum Press.

SPILLER, E. & ROSENBLUTH, A. E. (1986). *Opt. Eng.* **25**, 954–963.

SPILLER, E., SEGMÜLLER, A., RIFE, J. & HAELBICH, R.-P. (1980). *Appl. Phys. Lett.* **37**, 1048–1050.

TAPFER, L. & PLOOG, K. (1986). *Phys. Rev. B*, **33**, 5565–5574.

UNDERWOOD, J. H. & BARBEE, T. W. (1981). *Appl. Opt.* **20**, 3027–3034.

VIDAL, B. & VINCENT, P. (1984). *Appl. Opt.* **23**, 1794–1801.

ZIEGLER, E., LEPETRE, Y., SCHULLER, I. K. & SPILLER, E. (1986). *Appl. Phys. Lett.* **48**, 1354–1356.